Enhanced nonlinear susceptibility via double-double electromagnetically induced transparency

Hessa M. M. Alotaibi[1,2,*] and Barry C. Sanders[2,3,4,5]

[1]*Public Authority for Applied Education and Training, P.O. Box 23167, Safat 13092, Kuwait*

[2]*Institute for Quantum Science and Technology, University of Calgary, Calgary, Alberta, Canada T2N 1N4*

[3]*Hefei National Laboratory for Physical Sciences at Microscale, University of Science and Technology of China, CAS, Hefei 230026, China*

[4]*Shanghai Branch, CAS Center for Excellence and Synergetic Innovation Center in Quantum Information and Quantum Physics, University of Science and Technology of China, Shanghai 201305, 2015, China*

[5]*Program in Quantum Information Science, Canadian Institute for Advanced Research, Toronto, Ontario, Canada M5G 1Z8*

(Received 5 April 2016; published 16 November 2016)

We investigate the nonlinear optical susceptibility of an alkali-metal atom with tripod electronic configuration responsible for generating cross-phase modulation and self-phase modulation under the condition of double-double electromagnetically induced transparency. Our investigation demonstrates an enhancement in the nonlinear optical susceptibility of an alkali-metal atom by a factor of 1000 in the region of the second transparency window. This enhancement is in comparison with the atom's susceptibility in the first transparency window for the same parameters under the same conditions. Nonlinear-absorption enhancement arises by canceling Raman-gain generation, which arises when the probe and signal fields have equal intensities. At the center of the second transparency window, we obtain the condition required to attain a nonvanishing nonlinear optical susceptibility. In the bare-state picture, the coupling field must be off resonant from a bare-to-bare-state transition, while working in the semiclassical dressed picture required the signal field to be tuned off resonantly with a bare-to-dressed-state transition. The relation that governs the values of coupling- and signal-field detuning are also obtained. Our scheme exhibits the fact that the second transparency window has advantages over the first transparency window with respect to obtaining an enhanced Kerr effect, and our calculation includes simulation of both low-temperature and Doppler-broadened regimes.

DOI: 10.1103/PhysRevA.94.053832

I. INTRODUCTION

Electromagnetically induced transparency (EIT) is mainly a physical technique implemented to allow the transmission of electromagnetic radiation without any absorption [1] by removing the influence of an optical medium on propagating electromagnetic radiation. However, the power of EIT extends to improve generation of several optical processes, such as stimulated Raman gain [2] and lasing without inversion [3–8], and to enhance the efficiency of other precesses, such as frequency conversion [9], frequency-wave mixing, and parametric gain nonlinear processes [10–12], in addition to allowing the storage and slowing of light [13–17].

Another beneficial effect of EIT in the field of nonlinear optics includes enhancing the efficiency of the optical Kerr effect [18–21]. The Kerr effect is responsible for producing self-phase modulation (SPM) [22] and cross-phase modulation (XPM) required for many optical applications in the fields of quantum optics and quantum information, such as the implementation of optical shutters [23], quantum phase gates [24,25], quantum switches [26], optical solitons [27,28], and quantum nondemolition measurements [29]. These examples show that various EIT schemes have been suggested for producing the requisite optical Kerr nonlinearity to realize such phenomena [16,23–25,30–33]. The generation of optical Kerr nonlinearity under EIT conditions encounters an obstacle, the vanishing of the optical Kerr effect at the center of EIT window where absorption is minimal. In this case, the Kerr effect is obtained in the region surrounding the center of the EIT window, in which the XPM and SPM have a nonzero value but the absorption is high [16,24,25,31–33].

In this work, we present novel features of the tripod (⫛) atom-field configuration shown in Fig. 1. We show that operating the ⫛ atom-field configuration under the double-double electromagnetically induced transparency (DDEIT) condition significantly enhances the Kerr effect and produces a nonzero value of XPM and SPM at the center of the second EIT window where one-photon absorption is minimal for both the probe and signal fields. Unlike the N-scheme case [23], for which XPM is limited by temporal walk-off, resulting in different probe-field and signal-field group velocities, our proposed technique ensures further enhancement of the cross-Kerr effect by matching the group velocity of the probe and signal fields under the DDEIT condition.

DDEIT has been introduced using the ⫛ scheme [2] shown in Fig. 1(a). DDEIT exhibits DEIT for both the first EIT windows of the signal and probe and also the second windows. This optical system can be operated at either the first or the second window. The first window occurs at equal detunings of the probe, coupling, and signal fields. The second window is observed when the weak-field detunings are equal but different from the coupling-field detuning. The group velocities of the probe and signal fields can be matched in either the first or the second pair of transparency windows.

In this paper, we theoretically investigate the nonlinear interaction between the two fields under the DDEIT condition, i.e., when probe- and signal-field detunings are equal but different from the coupling-field detuning. Our result exhibits considerable enhancement in the third-order nonlinear optical susceptibilities, which improves the Kerr effect at the region of the second window.

*hmm.alotaibi@paaet.edu.kw

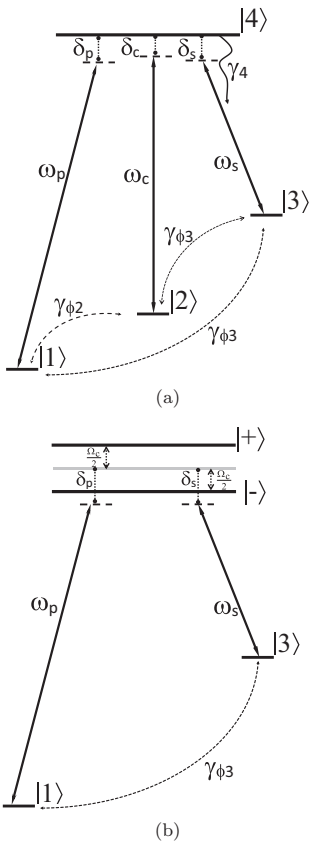

FIG. 1. Four-level ⫛-electronic structure with high-energy state $|4\rangle$ and lower-energy levels $|1\rangle$, $|2\rangle$, and $|3\rangle$ in ascending order in energy. Transitions are driven by probe (p), coupling (c), and signal (s) fields with frequencies ω_x and detunings δ_x with $x \in \{p,c,s\}$. Dephasing rates are $\gamma_{\phi i}$ for $i \in \{2,3\}$. (b) Same atom in the semiclassical dressed-state picture for strong c field in resonance with the $|2\rangle \leftrightarrow |4\rangle$ transition. Levels $|2\rangle$ and $|4\rangle$ are hybridized into $|\pm\rangle$.

Nonlinear optical susceptibilities are improved 1000-fold compared to their values in the region of the first EIT window under the same conditions. For a nonresonant coupling-field frequency, we attain a nonzero value of the nonlinear optical susceptibilities at the center of the second window, and their values are controlled by the coupling-field detuning. Moreover, in our proposed system the one- and two-photon absorptions of the signal and the probe fields vanish at the center of the second EIT window. The two-photon absorption at the center of the second window is canceled by Raman gain for equal field intensities [2].

Our work is presented in the following order. In Sec. II, we use the optical density-matrix elements describing the optical properties of the transitions $|1\rangle \rightarrow |4\rangle$ and $|3\rangle \rightarrow |4\rangle$ to determine the optical susceptibility of the probe and signal fields, respectively. We use these results to calculate the effective optical susceptibility up to third order in Sec. III. In this section, we present a detailed description of the self-action and cross-coupling Kerr effect. The influence of the coupling field on the dispersion properties of the probe field is discussed in Sec. IV, while Sec. V discusses the influence of Doppler broadening due to temperature increase on the optical susceptibility. Finally, we conclude in Sec. VI.

II. ATOMIC-OPTICAL SUSCEPTIBILITY

Consider the closed ⫛ atom-field model scheme depicted in Fig. 1 [2]. The lower electronic levels $|1\rangle$, $|2\rangle$, and $|3\rangle$ are coupled to the upper level $|4\rangle$ by three coherent fields, namely, the probe, coupling, and signal Rabi frequencies, Ω_p, Ω_c, and Ω_s, respectively. The electronic transitions $|1\rangle \leftrightarrow |2\rangle$, $|1\rangle \leftrightarrow |3\rangle$, and $|2\rangle \leftrightarrow |3\rangle$ are dipole forbidden. The three fields are detuned from the $|\imath\rangle \leftrightarrow |\jmath\rangle$ electronic transition frequency $\omega_{\imath\jmath}$ by

$$\delta_p := \omega_{41} - \omega_p, \quad \delta_c := \omega_{42} - \omega_c, \quad \delta_s := \omega_{43} - \omega_p, \tag{1}$$

respectively.

The analytical steady-state density-matrix elements used to find the probe-field effective optical susceptibility

$$\chi_p = \eta_p \frac{\rho_{14}}{\Omega_p}, \quad \eta_p = \frac{\mathcal{N}|\boldsymbol{d}_{41}|^2}{\epsilon_0 \hbar} \tag{2}$$

and the signal field effective optical susceptibility

$$\chi_s = \eta_s \frac{\rho_{34}}{\Omega_s}, \quad \eta_s = \frac{\mathcal{N}|\boldsymbol{d}_{43}|^2}{\epsilon_0 \hbar} \tag{3}$$

are [2]

$$\rho_{14} = i\Omega_p \frac{(\rho_{11}-\rho_{44})\left(\Gamma_{43} + 2i\delta_s + \frac{|\Omega_c|^2}{\Gamma_{32}+2i\delta_{sc}}\right) + (\rho_{11}-\rho_{44})\frac{|\Omega_p|^2}{\gamma_3-2i\delta_{ps}} + (\rho_{44}-\rho_{33})\frac{|\Omega_s|^2}{\gamma_3-2i\delta_{ps}}}{\left(\Gamma_{43} + 2i\delta_s + \frac{|\Omega_c|^2}{\Gamma_{32}+2i\delta_{sc}}\right)\left(\gamma_4 - 2i\delta_p + \frac{|\Omega_c|^2}{\gamma_2-2i\delta_{pc}} + \frac{|\Omega_s|^2}{\gamma_3-2i\delta_{ps}}\right) + \frac{|\Omega_p|^2}{\gamma_3-2i\delta_{ps}}\left(\gamma_4 - 2i\delta_p + \frac{|\Omega_c|^2}{\gamma_2-2i\delta_{pc}}\right)} \tag{4}$$

and

$$\rho_{34} = i\Omega_s \frac{(\rho_{33}-\rho_{44})\left(\gamma_4 + 2i\delta_p + \frac{|\Omega_c|^2}{\gamma_2+2i\delta_{sc}}\right) + (\rho_{33}-\rho_{44})\frac{|\Omega_s|^2}{\gamma_3+2i\delta_{ps}} + (\rho_{44}-\rho_{11})\frac{|\Omega_p|^2}{\gamma_3+2i\delta_{ps}}}{\left(\Gamma_{43} - 2i\delta_s + \frac{|\Omega_c|^2}{\Gamma_{32}-2i\delta_{sc}} + \frac{|\Omega_p|^2}{\gamma_3+2i\delta_{ps}}\right)\left(\gamma_4 + 2i\delta_p + \frac{|\Omega_c|^2}{\gamma_2+2i\delta_{pc}}\right) + \frac{|\Omega_s|^2}{\gamma_3+2i\delta_{ps}}\left(\Gamma_{43} - 2i\delta_s + \frac{|\Omega_c|^2}{\Gamma_{32}-2i\delta_{pc}}\right)}, \tag{5}$$

respectively, with $\mathcal{N}$ being the atomic density and $\boldsymbol{d}_{14}$ and $\boldsymbol{d}_{34}$ being the electric dipole moments of the $|1\rangle \leftrightarrow |4\rangle$ and $|3\rangle \leftrightarrow |4\rangle$ transitions, respectively. See Appendixes A, B, and C for detailed calculations of the steady-state solution of the density-matrix elements. Equations (4) and (5) are symmetric with respect to the $\delta_p \leftrightarrow \delta_s$ and $\rho_{11} \leftrightarrow \rho_{33}$ exchanges, which ensures identical dispersive and absorptive properties of the probe and signal fields for $\delta_p = \delta_s$ and $\rho_{11} = \rho_{33}$.

Subsequently, in the main part of the paper we consider the probe-field case, and the details concerning the signal-field nonlinear properties, which are similar, are discussed in Appendix D.

The quantities in Eq. (4) are the two-photon detuning

$$\delta_{xy} := \delta_x - \delta_y, \tag{6}$$

the coherence decay rate

$$\gamma_j := \sum_{i<j} (\gamma_{ji} + \gamma_{\phi j}), \tag{7}$$

with γ_{ji} being the decay rate from state $|j\rangle \to |i\rangle$ and $\gamma_{\phi i}$ being the dephasing of state $|i\rangle$, and the total coherence decay rate

$$\Gamma_{kl} = \gamma_k + \gamma_l. \tag{8}$$

The dephasing rate between the forbidden transitions is not zero [16]; therefore, $\gamma_2 = \gamma_{\phi 2}$ and $\gamma_3 = \gamma_{\phi 3}$.

In our system, the population in each state is highly dependent on the strength of the applied field, as discussed in detail in Appendix B of Ref. [17]. However, under the DDEIT condition, atoms are trapped in a dark state, which is a superposition of bare states $|1\rangle$ and $|3\rangle$. For the case that each of the probe and signal fields have the same strength or are close to each other in strength (which is our interest in this study), the populations satisfy $\rho_{11} \approx \rho_{33} \approx 0.5$, which implies that $\rho_{22} \approx \rho_{44} \approx 0$ [17]. For unequal probe- and signal-field Rabi frequencies, equal population can be maintained by incoherent excitation from the ground state $|1\rangle$ to the excited state $|4\rangle$ with constant pumping rate r [17] or maintained by transfer of population (ToP) between levels through spin-exchange collisions [34,35].

We verify the power of operating the $\Uparrow$ configuration at the second DEIT window by applying our calculation to alkali-metal atoms. Specifically, we consider ^{87}Rb and assign $|1\rangle$, $|2\rangle$, and $|3\rangle$ to the $5S_{1/2}$ level with

$$F = 1,\ m_F = 0 \tag{9}$$

and

$$F = 2,\ m_F = \{0, -2\}, \tag{10}$$

respectively. Level $|4\rangle$ corresponds to the $5P_{1/2}$ level with $F = 2$ and $m_F = -1$. The atom is driven by copropagating circularly polarized probe and signal fields, with the probe field driving the σ^- transition and the signal field driving the σ^+ transition. The decay rates from the upper-level coupling-field strength and the field detuning are assumed to be of the same order of magnitude.

III. NONLINEAR OPTICAL SUSCEPTIBILITY

In our investigation we are interested in studying the nonlinear interaction between the probe and signal fields that yields the cross-coupling effect, as well as studying the high-order nonlinearity that yields the self-action Kerr effect. Therefore, we keep terms up to third order of the nonlinear optical susceptibility. In this section, we consider the probe-field optical properties, whereas the signal-field case is discussed in Appendix D.

The effective optical susceptibility can be written using Eqs. (4) and (2) as

$$\chi_p = \chi_p^{(1)} + \chi_{p_{SPM}}^{(3)} |\boldsymbol{E}_p|^2 + \chi_{p_{XPM}}^{(3)} |\boldsymbol{E}_s|^2, \tag{11}$$

where

$$\chi_p^{(1)} = \frac{i\eta_p(\rho_{11} - \rho_{44})}{\gamma_4 - 2i\delta_p + \frac{|\Omega_c|^2}{\gamma_2 - 2i\delta_{pc}} + \frac{|\Omega_s|^2}{\gamma_3 - 2i\delta_{ps}}} \tag{12}$$

is the linear optical susceptibility at the probe-field frequency. The imaginary and real parts of the linear optical susceptibility are plotted in Figs. 2(a) and 2(b), respectively. The absorption and dispersion vanish at $\delta_p = \delta_c$, the center of the first EIT window, and at $\delta_p = \delta_s$, the center of the second EIT window.

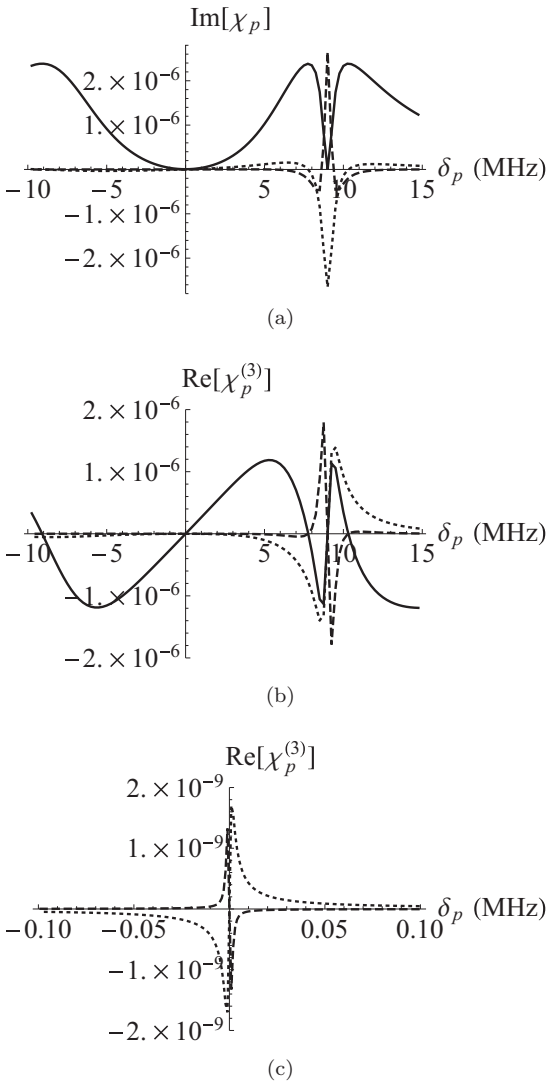

FIG. 2. (a) Im[χ_p] and (b) Re[χ_p] as a function of the probe-field detuning δ_p. The XPM term is represented by the dotted line, the SPM term is shown by the dashed line, and the linear term $\chi_p^{(1)} \times 10^{-3}$ is shown by the solid line, with $\gamma_4 = 18$ MHz, $\Omega_s = 0.2\gamma_4$, $\Omega_c = \gamma_4$, $\gamma_3 = 1$ kHz, $\gamma_2 = 40$ kHz, $\delta_s = 9$ MHz, $\delta_c = 0$, $d_{14} = d_{34} = 1.269 \times 10^{-29}$ C m, and $\mathcal{N} = 10^{12}$cm^{-3}. (c) Re[$\chi_p^{(3)}$] with XPM (dotted line) and SPM (dashed line) at the first EIT window when $\delta_c = 0$.

The second term of Eq. (11) represents the nonlinear optical process by the probe field with

$$\chi^{(3)}_{\mathrm{p_{SPM}}} = \frac{i\eta_{\mathrm{p_1}}(\rho_{11}-\rho_{44})}{(\gamma_3 - 2i\delta_{\mathrm{ps}})\left(\Gamma_{43} + 2i\delta_{\mathrm{s}} + \frac{|\Omega_{\mathrm{c}}|^2}{\Gamma_{32}+2i\delta_{\mathrm{sc}}}\right)} \times \frac{1 - \frac{\gamma_4 - 2i\delta_{\mathrm{p}} + \frac{|\Omega_{\mathrm{c}}|^2}{\gamma_2 - 2i\delta_{\mathrm{pc}}}}{\gamma_4 - 2i\delta_{\mathrm{p}} + \frac{|\Omega_{\mathrm{c}}|^2}{\gamma_2-2i\delta_{\mathrm{pc}}} + \frac{|\Omega_{\mathrm{s}}|^2}{\gamma_3-2i\delta_{\mathrm{ps}}}}}{\gamma_4 - 2i\delta_{\mathrm{p}} + \frac{|\Omega_{\mathrm{c}}|^2}{\gamma_2-2i\delta_{\mathrm{pc}}} + \frac{|\Omega_{\mathrm{s}}|^2}{\gamma_3-2i\delta_{\mathrm{ps}}}}, \tag{13}$$

which is the third-order nonlinear optical susceptibility, and

$$\eta_{\mathrm{p_1}} = \frac{\mathcal{N}|\boldsymbol{d}_{41}|^4}{\hbar^3\epsilon_0}. \tag{14}$$

The imaginary part of the second term characterizes the two-photon absorption of the probe field, whereas the real part describes the modulation of the field dispersion by the field self-action, called the self-Kerr effect [36]. The imaginary and real parts of $\chi^{(3)}_{\mathrm{p_{SPM}}}$ are shown by the dashed line in Figs. 2(a) and 2(b), respectively. The phase modulation of the probe field through the optical system by its self-action, i.e., SPM, can be calculated using [36]

$$\phi_{\mathrm{NL_{pSPM}}} = \frac{\omega_{\mathrm{p}}}{c} n_{\mathrm{p_{SPM}}} |\boldsymbol{E}_{\mathrm{p}}|^2 z_{\mathrm{p}}, \tag{15}$$

with

$$n_{\mathrm{p_{SPM}}} = \frac{\mathrm{Re}\left[\chi^{(3)}_{\mathrm{p_{SPM}}}\right]}{2n_{\mathrm{p}}}, \tag{16}$$

which is the second-order nonlinear refractive index [36]. Here z_{p} is the propagation distance of the probe field through the optical medium, and

$$n_{\mathrm{p}} \approx 1 + \tfrac{1}{2}\mathrm{Re}\left[\chi^{(1)}_{\mathrm{p}}\right] \tag{17}$$

is the linear index of refraction.

The third term in Eq. (11) depicts the cross-coupling effect between the probe and signal fields. The imaginary part of this term is responsible for producing stimulated Raman gain [2] for $\delta_{\mathrm{s}} = \delta_{\mathrm{p}}$. The real part represents the cross-coupling Kerr effect between the signal and probe fields, with the nonlinear optical susceptibility equal to

$$\chi^{(3)}_{\mathrm{p_{XPM}}} = \frac{i\eta_{\mathrm{sp}}(\rho_{44}-\rho_{33})}{(\gamma_3 - 2i\delta_{\mathrm{ps}})\left(\Gamma_{43} + 2i\delta_{\mathrm{s}} + \frac{|\Omega_{\mathrm{c}}|^2}{\Gamma_{32}+2i\delta_{\mathrm{sc}}}\right)} \times \frac{1}{\gamma_4 - 2i\delta_{\mathrm{p}} + \frac{|\Omega_{\mathrm{c}}|^2}{\gamma_2-2i\delta_{\mathrm{pc}}} + \frac{|\Omega_{\mathrm{s}}|^2}{\gamma_3-2i\delta_{\mathrm{ps}}}} \tag{18}$$

and

$$\eta_{\mathrm{sp}} = \frac{\mathcal{N}|\boldsymbol{d}_{41}|^2|\boldsymbol{d}_{43}|^2}{\hbar^3\epsilon_0}. \tag{19}$$

The modulation of the probe-field phase by the signal-field intensity through the nonlinear medium can be obtained using [36]

$$\phi_{\mathrm{NL_{pXPM}}} = \frac{\omega_{\mathrm{p}}}{c} n_{\mathrm{p_{XPM}}} |\boldsymbol{E}_{\mathrm{s}}|^2 z_{\mathrm{p}}, \tag{20}$$

where

$$n_{\mathrm{p_{XPM}}} = \frac{\mathrm{Re}\left[\chi^{(3)}_{\mathrm{p_{XPM}}}\right]}{2n_{\mathrm{p}}} \tag{21}$$

is the second-order nonlinear refractive index associated with the cross-coupling effect.

The two-photon absorption of the probe field described by the imaginary part of the second term in Eq. (11) is compensated by stimulated Raman gain described by the imaginary part of the third term of Eq. (11). When $\Omega_{\mathrm{p}} = \Omega_{\mathrm{s}}$, the absorption is canceled by the Raman gain in the system. This has the advantage of obtaining XPM and SPM not accompanied by nonlinear absorption, as shown in Fig. 2(a).

The variation of $\mathrm{Re}[\chi^{(3)}]$ constitutes the variation of the SPM and XPM, as evidenced by Eqs. (15) and (20), respectively. Referring to Fig. 2(b), the value of $\mathrm{Re}[\chi^{(3)}]$ vanishes at the center of the two transparency windows, i.e., when $\delta_{\mathrm{p}} = \delta_{\mathrm{c}}$ and $\delta_{\mathrm{p}} = \delta_{\mathrm{s}}$. However, the value of $\mathrm{Re}[\chi^{(3)}]$ in the region of the second window is greatly enhanced compared to its value in the region of the first window.

The maximum of $\mathrm{Re}[\chi^{(3)}]$ at the region of the second window exceeds its value in the region of the first window by a factor of 1000, as seen by comparing Fig. 2(b) with Fig. 2(c). The enhancement in the nonlinear optical susceptibility exhibits the potential of operating the Λ atom-field scheme in the second EIT window compared to the first EIT window.

IV. VARIATION OF THE PROBE-FIELD NONLINEAR INDEX OF REFRACTION BY THE APPLIED FIELD DETUNINGS

Coupling-field detuning is influential for improving SPM and XPM performance values at the center of the second window. Figure 3 demonstrates the variation of $\mathrm{Re}[\chi^{(3)}]$ as a function of the coupling-field detuning. The nonlinear optical dispersion response vanishes when the coupling field is in resonance with the $|2\rangle \leftrightarrow |4\rangle$ transition. It also vanishes when the coupling-field detuning is equal to the signal-field detuning in which the optical system is operated at the center of the first window. Tuning the coupling field to a lower or higher energy than the $|2\rangle \leftrightarrow |4\rangle$ transition energy displaces the values of the $\mathrm{Re}[\chi^{(3)}]$ from zero. Then $|i\rangle\,\mathrm{Re}[\chi^{(3)}]$ reaches the maximum values when $\delta_{\mathrm{c}} = \frac{\delta_{\mathrm{s}}}{2}$.

In the analysis that follows, we investigate further the real part of $\chi^{(3)}_{\mathrm{p_{XPM}}}$ to determine the condition required to attain a nonzero value when $\delta_{\mathrm{p}} = \delta_{\mathrm{s}}$. From Eq. (18),

$$\mathrm{Re}\left[\chi^{(3)}_{\mathrm{p_{XPM}}}\right] = \frac{2\eta_{\mathrm{sp}}(\rho_{44}-\rho_{33})\left[\left(\delta_{\mathrm{s}} - \frac{|\Omega_{\mathrm{c}}|^2\delta_{\mathrm{sc}}}{\Gamma_{32}^2+4\delta_{\mathrm{sc}}^2}\right)\left(\gamma_4 + \frac{|\Omega_{\mathrm{c}}|^2\gamma_2}{\gamma_2^2+4\delta_{\mathrm{pc}}^2} + \frac{|\Omega_{\mathrm{s}}|^2}{\gamma_3}\right) + \left(\frac{|\Omega_{\mathrm{c}}|^2\delta_{\mathrm{pc}}}{\gamma_2^2+4\delta_{\mathrm{pc}}^2} - \delta_{\mathrm{p}}\right)\left(\Gamma_{43} + \frac{|\Omega_{\mathrm{c}}|^2\Gamma_{32}}{\Gamma_{32}^2+4\delta_{\mathrm{sc}}^2}\right)\right]}{\gamma_3\left[\left(\gamma_4 + \frac{|\Omega_{\mathrm{c}}|^2\gamma_2}{\gamma_2^2+4\delta_{\mathrm{pc}}^2} + \frac{|\Omega_{\mathrm{s}}|^2}{\gamma_3}\right)^2 + 4\left(\frac{|\Omega_{\mathrm{c}}|^2\delta_{\mathrm{pc}}}{\gamma_2^2+4\delta_{\mathrm{pc}}^2} - \delta_{\mathrm{p}}\right)^2\right]\left[\left(\Gamma_{43} + \frac{|\Omega_{\mathrm{c}}|^2\Gamma_{32}}{\Gamma_{32}^2+4\delta_{\mathrm{sc}}^2}\right)^2 + 4\left(\delta_{\mathrm{s}} - \frac{|\Omega_{\mathrm{c}}|^2\delta_{\mathrm{sc}}}{\Gamma_{32}^2+4\delta_{\mathrm{sc}}^2}\right)^2\right]}, \tag{22}$$

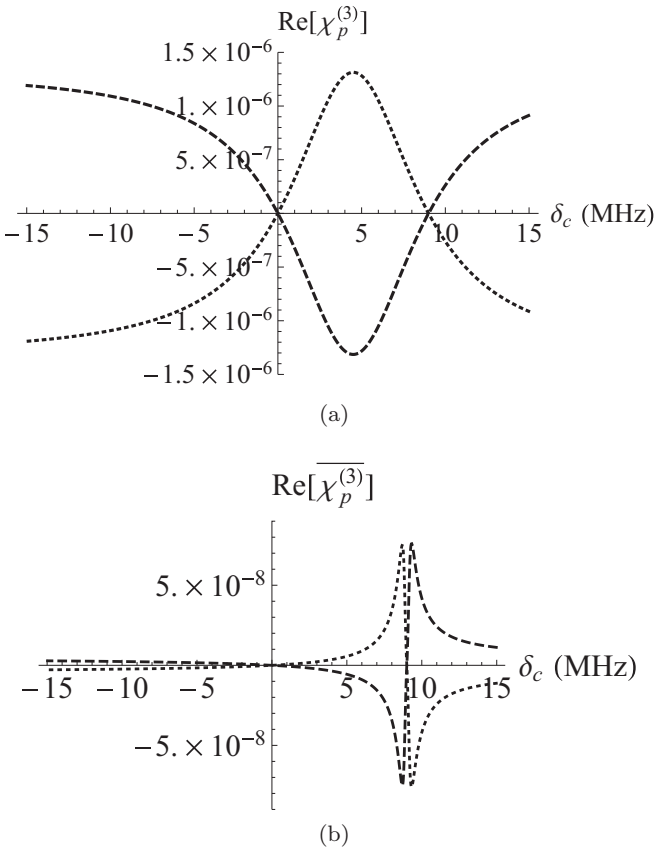

FIG. 3. (a) $\mathrm{Re}[\chi_{\mathrm{p}}^{(3)}]$ with XPM (dotted line) and SPM (dashed line) as a function of the coupling-field detuning δ_{c} at the center of the second EIT window when $\delta_{\mathrm{s}} = \delta_{\mathrm{p}} = 9$ MHz. (b) Same as (a), but under the Doppler broadening effect at $T = 300$ K. Other parameters are $\gamma_4 = 18$ MHz, $\Omega_{\mathrm{s}} = 0.2\gamma_4$, $\Omega_{\mathrm{c}} = \gamma_4$, $\gamma_3 = 10$ kHz, $\gamma_2 = 40$ kHz, $d_{14} = d_{34} = 1.269 \times 10^{-29}$ C m, and $\mathcal{N} = 10^{12}\,\mathrm{cm}^{-3}$.

where η_{sp} is defined by (19). Our earlier assumption of having a coupling-field strength and field detunings of the same order of magnitude, in addition to having a low dephasing, as in our optical system using ^{87}Rb gas [16], simplifies Eq. (22) to

$$\mathrm{Re}\left[\chi_{\mathrm{p_{XPM}}}^{(3)}\right] \approx \frac{2\eta_{\mathrm{sp}}(\rho_{44}-\rho_{33})\delta_{\mathrm{sc}}^2\left(\delta_{\mathrm{s}} - \frac{|\Omega_{\mathrm{c}}|^2}{4\delta_{\mathrm{sc}}}\right)}{|\Omega_{\mathrm{s}}|^2\left[\delta_{\mathrm{sc}}^2\Gamma_{43}^2 + 4\left(\delta_{\mathrm{sc}}\delta_{\mathrm{s}} - \frac{|\Omega_{\mathrm{c}}|^2}{4}\right)^2\right]}. \tag{23}$$

Equation (23) vanishes when $\delta_{\mathrm{s}} = \delta_{\mathrm{c}}$ and for

$$\delta_{\mathrm{s}} - \frac{|\Omega_{\mathrm{c}}|^2}{4\delta_{\mathrm{sc}}} = 0. \tag{24}$$

Under the DDEIT condition, $\delta_{\mathrm{s}} \neq \delta_{\mathrm{c}}$ is always true. Therefore, the XPM vanishes only whenever (24) is satisfied. In other words, the condition

$$\delta_{\mathrm{s}} - \delta_{\mathrm{c}} \neq \frac{|\Omega_{\mathrm{c}}|^2}{4\delta_{\mathrm{s}}} \tag{25}$$

is mandatory to obtain a nonzero value for $n_{\mathrm{p_{XPM}}}$ at the center of the second window. When the coupling field is in resonance with the $|2\rangle \leftrightarrow |4\rangle$ transition, condition (25) changes to

$$\left(\delta_{\mathrm{s}} - \frac{|\Omega_{\mathrm{c}}|}{2}\right)\left(\delta_{\mathrm{s}} + \frac{|\Omega_{\mathrm{c}}|}{2}\right) \neq 0. \tag{26}$$

In the semiclassical dressed model of the $\Uparrow$ scheme [2], the dressed states $|\pm\rangle$ are shifted from the $|2\rangle \leftrightarrow |4\rangle$ transition by $\omega_{\pm}$ depending on the coupling-field detuning value,

$$\omega_{\pm} = \frac{\delta_{\mathrm{c}} \pm R}{2}, \quad R := \sqrt{|\Omega_{\mathrm{c}}|^2 + \delta_{\mathrm{c}}^2}. \tag{27}$$

For a resonant coupling field, the dressed states $|\pm\rangle$ are shifted by $\pm\frac{|\Omega_{\mathrm{c}}|}{2}$, as shown in Fig. 1(b). Detuning the signal field by $\pm\frac{|\Omega_{\mathrm{c}}|}{2}$ leads to resonance of the field with the $|3\rangle \leftrightarrow |\mp\rangle$ transition.

According to condition (26), $n_{\mathrm{p_{XPM}}}$ vanishes when the signal field is in resonance with the $|3\rangle \leftrightarrow |\pm\rangle$ transition. Therefore, the signal field must be detuned off resonantly from the $|3\rangle \leftrightarrow |\pm\rangle$ transition to attain a nonzero value for $n_{\mathrm{p_{XPM}}}$. This is equivalent to displacing the second window from being centered at the absorption peak of the $|1\rangle \leftrightarrow |\pm\rangle$ transition. The above results can be generalized to involve the case of SPM as analyzing $\mathrm{Re}[\chi_{\mathrm{p_{SPM}}}^{(3)}]$ leads to the same result as above.

For the case shown in Fig. 2, the coupling field has been selected to be in resonance with the $|2\rangle \leftrightarrow |4\rangle$ transition, whereas the signal field was chosen to be in resonance with the transition $|3\rangle \leftrightarrow |-\rangle$, i.e., $\delta_{\mathrm{s}} = \frac{\Omega_{\mathrm{c}}}{2}$ [2]. Our choice of frequency detuning centers the second EIT window at the absorption peak of the $|1\rangle \rightarrow |-\rangle$ transition and compels the nonlinear index of refraction to fade at the center of the second window. We can avoid the zero nonlinear index of refraction by changing the signal-field detuning to satisfy condition (26).

To summarize, our condition (25) quantifies the requirement for our system to enhance the Kerr effect in terms of bare and dressed states. For a resonant coupling field, the signal field must be off-resonant from the dressed-state transition $|3\rangle \leftrightarrow |\pm\rangle$. The enhancement of the nonlinear index of refraction can be explained due to the Stark shift [31]. The off-resonant coupling field from transition $|2\rangle \leftrightarrow |4\rangle$ and the signal field from transition $|3\rangle \leftrightarrow |\pm\rangle$ modifies the $\Uparrow$ scheme by producing an ac Stark shift for states $|2\rangle$ and $|3\rangle$, respectively.

V. DOPPLER BROADENING EFFECT ON NONLINEAR OPTICAL SUSCEPTIBILITIES

In the following calculation, which accounts for the dependence on temperature T (where k is Boltzmann's constant) and on v, which is the velocity component in the direction of the three copropagating signal (s), probe (p), and coupling (c) fields, we use the subscript x to denote $\mathrm{x} \in \{\mathrm{p}, \mathrm{c}, \mathrm{s}\}$. Transition frequencies are expressed as

$$\omega_{\mathrm{x}} = \begin{cases} \omega_{14} \equiv \omega_0, & \mathrm{x} = \mathrm{p}, \\ \omega_{24}, & \mathrm{x} = \mathrm{c}, \\ \omega_{34}, & \mathrm{x} = \mathrm{s}. \end{cases} \tag{28}$$

We construct velocity-dependent susceptibility $\chi_{\mathrm{p}}(v)$ from Eqs. (13) and (18) by substituting [17] $\delta_{\mathrm{x}} \mapsto \delta_{\mathrm{x}} - v\omega_{\mathrm{x}}/c$. With these relations in place, we can determine the Doppler broadening effect by integrating susceptibilities (12), (13), and (18) according to [37]

$$\bar{\chi}_{\mathrm{p}} := \int_{-\infty}^{\infty} \chi_{\mathrm{p}}(v) f(v) dv \tag{29}$$

for the Maxwell-Boltzmann velocity distribution

$$f(v) = \frac{1}{u\sqrt{\pi}} \exp\left(-\frac{v^2}{u^2}\right),\ u = \sqrt{\frac{2kT}{m}}, \tag{30}$$

where m is the atomic mass.

We propose operating in the regime in which the co-propagating fields are driving approximately equal transition frequencies $\omega_0 \equiv \omega_{14} \approx \omega_{24} \approx \omega_{34}$, which allows the Doppler effect on two-photon detuning δ_{xy} (6) to be neglected. These restrictions on frequencies are commensurate with operating conditions for a ^{87}Rb gas. Therefore, the quantities $\{\delta_{xy}\}$ are substantially intact in Eqs. (13) and (18) due to temperature effects and thus do not change under Doppler broadening.

The complex optical susceptibility is evaluated numerically with the same parameters as in Fig. 2 but for room temperature (300 K). We display the results from this numerical simulation in Fig. 4. Comparing these figures shows a reduction of the EIT window width by an amount that is commensurate with past observations [38]. Despite Doppler broadening, both EIT windows are strongly evident, and the value of $\chi_p^{(3)}$ in the second window is clearly higher than its value in the first window with respect to Doppler broadening.

We can now see the effect of coupling-field detuning on SPM and XPM. As in the low-temperature limit, shifting the coupling-field detuning from resonance enhances SPM and XPM. However, the maximum is thus shifted from $\delta_c = \delta_s/2$ due to the Doppler effect, as depicted in Fig. 3(b).

VI. CONCLUSION

We have accomplished our objective of showing that the second DEIT window has an advantage over the first transparency window with respect to the goal of obtaining an enhanced Kerr effect. Operating a $\Uparrow$ atom-field configuration under a DDEIT condition significantly enhances the Kerr effect and generates nonzero values for $n_{p_{XPM}}$ and $n_{p_{SPM}}$ at the center of the second EIT window, where one-photon absorption is minimal for both the probe and signal fields. The enhancement of $n_{p_{XPM}}$ and $n_{p_{SPM}}$ leads to values 1000 times those in the region of the first EIT window under the same conditions. Detuning the coupling field from the $|2\rangle \leftrightarrow |4\rangle$ transition and detuning the signal field from the $|3\rangle \leftrightarrow |\pm\rangle$ transition produce an ac Stark shift for states $|2\rangle$ and $|3\rangle$, respectively, which modifies the $\Uparrow$ scheme and improves the nonlinear index of refraction at the center of the second EIT window. Mathematically, condition (25) must be attained in order to obtain nonzero values for $n_{p_{XPM}}$ and $n_{p_{SPM}}$ at the center of the second EIT window.

In our system two-photon absorption is canceled by Raman gain due to the high-order nonlinear interaction between probe and signal fields when the two fields have equal detuning from the atomic transition. Our proposed scheme, which aims to realize a high nonlinear phase shift, should be experimentally feasible as we have employed realistic parameters for ^{87}Rb, including dephasing, driving fields, and temperature.

APPENDIX A: ATOM-FIELD HAMILTONIAN

The Hamiltonian system that describes the coupling of four nondegenerate states by three coherent radiation fields shown

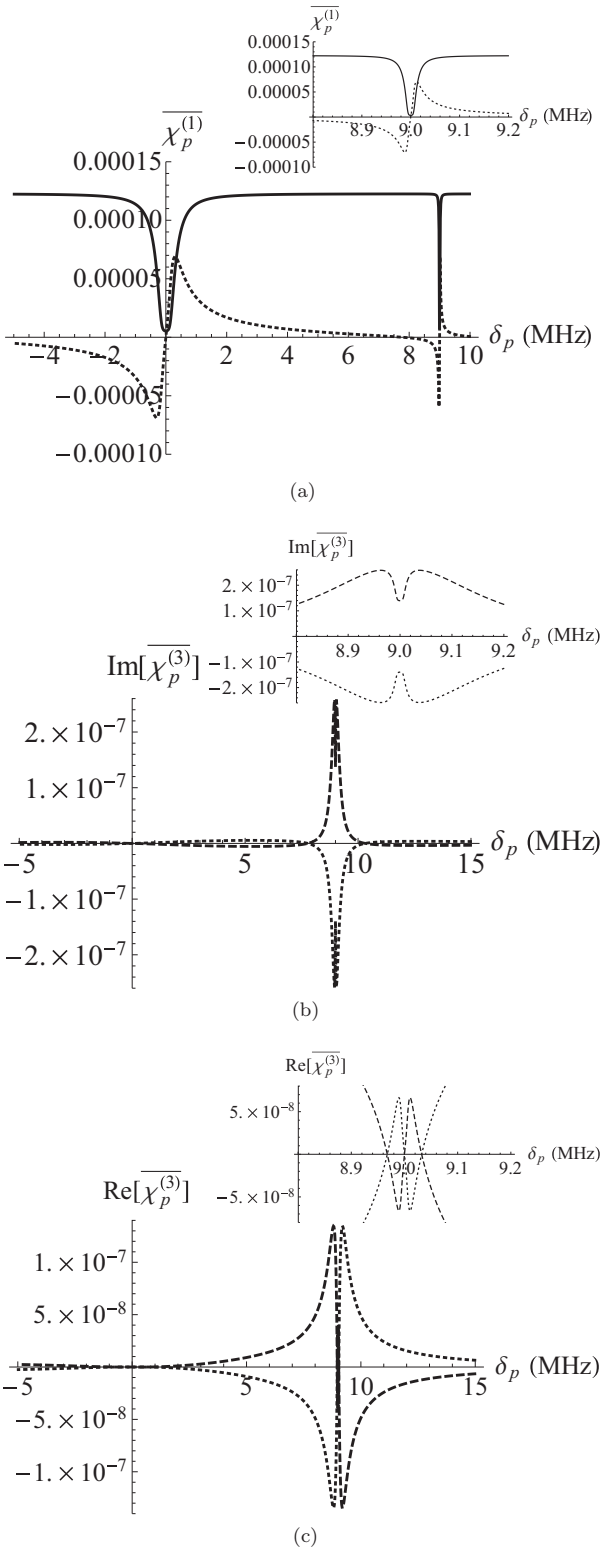

FIG. 4. Numerical plots of Doppler broadening Im$[\chi_p]$ and Re$[\chi_p]$ as a function of the probe-field detuning δ_p for the same parameters as in Fig. 2 but at $T = 300$ K. (a) Linear optical susceptibility, with Im$[\chi_p^{(1)}]$ (solid line) and Re$[\chi_p^{(1)}]$ (dotted line). (b) Im$[\chi_p^{(3)}]$ and (c) Re$[\chi_p^{(3)}]$ with XPM (dotted line) and SPM (dashed line). The insets show a magnification of (a), (b), and (c) around the region of the second EIT window.

in Fig. 1(a) is

$$\hat{H}(t) = \hat{H}_0 + \hat{H}_{\rm dr}(t), \tag{A1}$$

where $\hat{H}_0$ is the unperturbed part that represents the free-atom Hamiltonian,

$$\hat{H}_0 = \sum_{\imath=1}^{4} \hbar\omega_\imath |\imath\rangle\langle\imath|, \tag{A2}$$

with $\hat{H}_0|\imath\rangle = \hbar\omega_\imath|\imath\rangle$. States $|1\rangle$, $|2\rangle$, $|3\rangle$, and $|4\rangle$ are the eigenstates of the unperturbed part of $\hat{H}(t)$, with eigenvalues $\hbar\omega_1$, $\hbar\omega_2$, $\hbar\omega_3$, and $\hbar\omega_4$, respectively. The part of the Hamiltonian $\hat{H}_{\rm dr}(t)$ that represents the interaction of the atom with the radiation field $\boldsymbol{E}(t)$ polarized in the ε direction and propagated in the z direction can be written as

$$\hat{H}_{\rm dr}(t) = -\boldsymbol{d}\cdot\boldsymbol{E}(t), \tag{A3}$$

where $\boldsymbol{d}$ is the dipole moment and the electric field is represented by

$$\boldsymbol{E}(t) = \sum_{\mathrm{x}\in\{\mathrm{c,\,p,\,s}\}} \boldsymbol{E}_{\mathrm{x}}(t) = \frac{\sum_{\mathrm{x}} \xi_{\mathrm{x}} e^{i\omega_{\mathrm{x}}t}\hat{\varepsilon}_{\mathrm{x}} + \text{c.c.}}{2}, \tag{A4}$$

with $\hat{\varepsilon}_{\mathrm{x}}$ being the polarization vectors of a field of mode x, ξ_{x} being the amplitude envelope function of the field, and c.c. denoting the complex conjugate.

The summation in (A4) considers only positive frequency. These field modes comprise a coupling field of angular frequency ω_{c} interacting with a pair of states $|2\rangle \leftrightarrow |4\rangle$, a probe field of angular frequency ω_{p} coupling the transition $|1\rangle \leftrightarrow |4\rangle$, and a signal field of angular frequency ω_{s} coupling the transition $|3\rangle \leftrightarrow |4\rangle$, as shown in Fig. 1(a).

Inserting the identity

$$\mathbb{1} = |1\rangle\langle 1| + |2\rangle\langle 2| + |3\rangle\langle 3| + |4\rangle\langle 4| \tag{A5}$$

into Eq. (A3) yields

$$\begin{aligned}\hat{H}_{\rm dr}(t) =& -(|1\rangle\langle 1| + |2\rangle\langle 2| + |3\rangle\langle 3| + |4\rangle\langle 4|)\boldsymbol{d}(|1\rangle\langle 1| + |2\rangle\langle 2| + |3\rangle\langle 3| + |4\rangle\langle 4|)\cdot\boldsymbol{E}(t)\\ =& -[|1\rangle\langle 1|\boldsymbol{d}|4\rangle\langle 4|\cdot\boldsymbol{E}_{\mathrm{p}}(t) + |2\rangle\langle 2|\boldsymbol{d}|4\rangle\langle 4|\cdot\boldsymbol{E}_{\mathrm{c}}(t) + |3\rangle\langle 3|\boldsymbol{d}|4\rangle\langle 4|\cdot\boldsymbol{E}_{\mathrm{s}}(t)\\ &+ |4\rangle\langle 4|\boldsymbol{d}|1\rangle\langle 1|\cdot\boldsymbol{E}_{\mathrm{p}}(t) + |4\rangle\langle 4|\boldsymbol{d}|2\rangle\langle 2|\cdot\boldsymbol{E}_{\mathrm{c}}(t) + |4\rangle\langle 4|\boldsymbol{d}|3\rangle\langle 3|\cdot\boldsymbol{E}_{\mathrm{s}}(t)].\end{aligned} \tag{A6}$$

The frequency components of the coupling, probe, and signal fields are tuned close to resonance with respect to the one-photon transition. Therefore, the three nearly resonant electric fields are expected to affect only the transitions $|2\rangle \to |4\rangle$, $|1\rangle \to |4\rangle$, and $|3\rangle \to |4\rangle$, respectively. Thus, we can disregard off-resonance terms, and Eq. (A6) reduces to

$$\begin{aligned}\hat{H}_{\rm dr}(t) =& -(\boldsymbol{d}_{14}\cdot\hat{\varepsilon}_{\mathrm{p}}\hat{\sigma}_{14} + \boldsymbol{d}_{41}\cdot\hat{\varepsilon}_{\mathrm{p}}\hat{\sigma}_{41})\frac{\xi_{\mathrm{p}}e^{i\omega_{\mathrm{p}}t} + \text{c.c.}}{2}\\ &-(\boldsymbol{d}_{24}\cdot\hat{\varepsilon}_{\mathrm{c}}\hat{\sigma}_{24} + \boldsymbol{d}_{42}\cdot\hat{\varepsilon}_{\mathrm{c}}\hat{\sigma}_{42})\frac{\xi_{\mathrm{c}}e^{i\omega_{\mathrm{c}}t} + \text{c.c.}}{2}\\ &-(\boldsymbol{d}_{34}\cdot\hat{\varepsilon}_{\mathrm{s}}\hat{\sigma}_{34} + \boldsymbol{d}_{43}\hat{\cdot}\hat{\varepsilon}_{\mathrm{s}}\sigma_{43})\frac{\xi_{\mathrm{s}}e^{i\omega_{\mathrm{s}}t} + \text{c.c.}}{2},\end{aligned} \tag{A7}$$

where $\hat{\sigma}_{\imath\jmath} = |\imath\rangle\langle\jmath|$ is the projection operator and $\boldsymbol{d}_{\imath\jmath} = \boldsymbol{d}^*_{\jmath\imath} = \langle\imath|\boldsymbol{d}|\jmath\rangle$ are the dipole matrix elements of the $|\imath\rangle \leftrightarrow |\jmath\rangle$ transition for $\imath \neq \jmath$.

We assume that the transitions

$$|1\rangle \leftrightarrow |2\rangle,\ |1\rangle \leftrightarrow |3\rangle,\ |2\rangle \leftrightarrow |3\rangle \tag{A8}$$

are dipole-forbidden. Thus,

$$\boldsymbol{d}_{12} = \boldsymbol{d}_{23} = \boldsymbol{d}_{13} = 0. \tag{A9}$$

From the rotating-wave approximation,

$$\begin{aligned}\hat{H}_{\rm dr}(t) =& -\tfrac{1}{2}(\boldsymbol{d}_{14}\cdot\hat{\varepsilon}_{\mathrm{p}}\xi_{\mathrm{p}}e^{i\omega_{\mathrm{p}}t}\hat{\sigma}_{14} + \boldsymbol{d}_{24}\cdot\hat{\varepsilon}_{\mathrm{c}}\xi_{\mathrm{c}}e^{i\omega_{\mathrm{c}}t}\hat{\sigma}_{24}\\ &+ \boldsymbol{d}_{34}\cdot\hat{\varepsilon}_{\mathrm{s}}\xi_{\mathrm{s}}e^{i\omega_{\mathrm{s}}t}\hat{\sigma}_{34} + \text{H.c.}),\end{aligned} \tag{A10}$$

with H.c. denoting the Hermitian conjugate. We define the strength of the resonant interaction between the applied fields and the four-level atom by

$$\begin{aligned}\Omega_{\mathrm{c}} &= -\frac{\boldsymbol{d}_{24}\cdot\hat{\varepsilon}_{\mathrm{c}}\xi_{\mathrm{c}}}{\hbar},\\ \Omega_{\mathrm{s}} &= -\frac{\boldsymbol{d}_{34}\cdot\hat{\varepsilon}_{\mathrm{s}}\xi_{\mathrm{s}}}{\hbar},\end{aligned} \tag{A11}$$

which are known as the Rabi frequencies.

Thus, we write Eq. (A10) as

$$\hat{H}_{\rm dr}(t) = \frac{\hbar}{2}(\Omega_{\mathrm{p}}e^{i\omega_{\mathrm{p}}t}\sigma_{14} + \Omega_{\mathrm{c}}e^{i\omega_{\mathrm{c}}t}\sigma_{24} + \Omega_{\mathrm{s}}e^{i\omega_{\mathrm{s}}t}\sigma_{34} + \text{H.c.}). \tag{A12}$$

In the interaction picture, with respect to the free-atom Hamiltonian (A2), the atom-field system Hamiltonian has the form

$$\hat{V}(t) = \hat{U}^\dagger(t)\hat{H}_{\rm dr}(t)\hat{U}(t), \tag{A13}$$

with

$$\hat{U}(t) = e^{\frac{-i\hat{H}_0 t}{\hbar}} = \sum_{i=1}^{4} e^{-i\omega_i t}|i\rangle\langle i| \tag{A14}$$

being the unitary transformation operator, where we use the fact that the eigenstates of $\hat{H}_0$ are orthonormal (i.e., $\langle\imath|\jmath\rangle = 0$ for $\imath \neq \jmath$ and $\langle\imath|\imath\rangle = 1$) to obtain (A14). By substituting Eqs. (A12) and (A14) into Eq. (A13) we obtain

$$\hat{V}(t) = \frac{\hbar}{2}(\Omega_{\mathrm{p}}e^{-i\delta_{\mathrm{p}}t}\hat{\sigma}_{14} + \Omega_{\mathrm{c}}e^{-i\delta_{\mathrm{c}}t}\hat{\sigma}_{24} + \Omega_{\mathrm{s}}e^{-i\delta_{\mathrm{s}}t}\hat{\sigma}_{34} + \text{H.c.}), \tag{A15}$$

with δ_{x} defined in Eq. (1).

The atom-field system Hamiltonian described by Eq. (A15) involves terms oscillating at different optical frequencies. Thus, our next step is to find a Hermitian operator to transform the Hamiltonian to a rotating frame in order to eliminate the

time dependence [39]. The transformation that we apply is constructed to remove all time dependence from the interaction Hamiltonian.

This new basis is known as the rotating basis and is related to the old basis by

$$|\psi'\rangle = \hat{U}'(t)|\psi\rangle, \tag{A16}$$

with

$$\hat{U}'(t) = e^{\frac{-i\hat{A}t}{\hbar}}, \tag{A17}$$

where $\hat{A}$ is a self-adjoint operator. The corresponding transformed Hamiltonian $\hat{H}'$ for the transformed wave function $|\psi'\rangle$ can be found using

$$\hat{H}' = \hat{U}'(t)\hat{V}(t)\hat{U}'^{\dagger}(t) + \hat{A}. \tag{A18}$$

In the case of our atom-field system, the operator $\hat{A}$ used to eliminate the time dependence is

$$\hat{A} = 3\delta_{\rm p}\sigma_{11} + (2\delta_{\rm p} + \delta_{\rm c})\sigma_{22} + (2\delta_{\rm p} + \delta_{\rm s})\sigma_{33} + 2\delta_{\rm p}\sigma_{44}. \tag{A19}$$

The resultant Hamiltonian after transformation is [2]

$$\hat{H}' = \hat{H}'_0 + \frac{\hbar}{2}(\Omega_{\rm p}\hat{\sigma}_{14} + \Omega_{\rm c}\hat{\sigma}_{24} + \Omega_{\rm s}\hat{\sigma}_{34} + \text{H.c.}) \tag{A20}$$

for

$$\hat{H}'_0 := \delta_{\rm pc}\hat{\sigma}_{22} + \delta_{\rm ps}\hat{\sigma}_{33} + \delta_{\rm p}\hat{\sigma}_{44}, \tag{A21}$$

where we have added

$$3\delta_{\rm p}(\sigma_{11} + \sigma_{22} + \sigma_{33} + \sigma_{44}) \tag{A22}$$

to the transformed Hamiltonian to obtain $\hat{H}'$, which shifts the eigenvalue by $3\delta_{\rm p}$. This has no physical effect, as the physically relevant terms are the differences between energy levels.

APPENDIX B: OPEN-SYSTEM DYNAMICS AND DENSITY-MATRIX ELEMENTS

In the presence of damping, atomic dynamics and the state's time evolution are described by the density operator, which is governed by a master equation for the atomic density operator. The resulting Lindblad master equation is [2]

$$\dot{\rho} = -\frac{i}{\hbar}[\rho, \hat{H}'] + \sum_{\iota<\jmath}^{4}\frac{\gamma_{\jmath\iota}}{2}(\sigma_{\iota\jmath}\rho\sigma_{\jmath\iota} - \sigma_{\jmath\jmath}\rho - \rho\sigma_{\jmath\jmath}) + \sum_{\jmath=2}^{4}\frac{\gamma_{\phi\jmath}}{2}(\sigma_{\jmath\jmath}\rho\sigma_{\jmath\jmath} - \sigma_{\jmath\jmath}\rho - \rho\sigma_{\jmath\jmath}). \tag{B1}$$

The Lindblad master equation includes both spontaneous emissions and dephasing, where $\gamma_{\jmath\iota}$ is the decay rate of state $|\jmath\rangle \to |\iota\rangle$ and $\gamma_{\phi\iota}$ is the dephasing of state $|\iota\rangle$. By substituting Eq. (A20) into Eq. (B1) we obtain ten optical Bloch equations.

Six more optical Bloch equations are obtained from complex conjugates of the six off-diagonal density-matrix expressions,

$$\dot{\rho}_{12}(t) = \left(-\frac{1}{2}\gamma_2 + i\delta_{\rm pc}\right)\rho_{12}(t) - \frac{i}{2}[-\Omega_{\rm c}^*\rho_{14}(t) + \Omega_{\rm p}\rho_{24}(t)], \tag{B2}$$

$$\dot{\rho}_{13}(t) = \left(-\frac{1}{2}\gamma_3 + i\delta_{\rm ps}\right)\rho_{13}(t) - \frac{i}{2}[-\Omega_{\rm s}^*\rho_{14}(t) + \Omega_{\rm p}\rho_{43}(t)], \tag{B3}$$

$$\dot{\rho}_{14}(t) = \left(-\frac{1}{2}\gamma_4 + i\delta_{\rm p}\right)\rho_{14}(t) + \frac{i}{2}\{\Omega_{\rm c}\rho_{12}(t) + \Omega_{\rm s}\rho_{13}(t) + \Omega_{\rm p}[\rho_{11}(t) - \rho_{44}(t)]\}, \tag{B4}$$

$$\dot{\rho}_{23}(t) = \left(-\frac{1}{2}\Gamma_{32} - i\delta_{\rm sc}\right)\rho_{23}(t) - \frac{i}{2}\left[\Omega_{\rm c}\rho_{43}(t) - \Omega_{\rm s}^*\rho_{24}(t)\right], \tag{B5}$$

$$\dot{\rho}_{24}(t) = \left(-\frac{1}{2}\Gamma_{42} + i\delta_{\rm c}\right)\rho_{24}(t) - \frac{i}{2}\{-\Omega_{\rm p}\rho_{21}(t) + \Omega_{\rm c}[\rho_{44}(t) - \rho_{22}(t)] - \Omega_{\rm s}\rho_{23}(t)\}, \tag{B6}$$

$$\dot{\rho}_{43}(t) = \left(-\frac{1}{2}\Gamma_{43} - i\delta_{\rm s}\right)\rho_{43}(t) + \frac{i}{2}\{-\Omega_{\rm c}^*\rho_{23}(t) + \Omega_{\rm s}^*[\rho_{44}(t) - \rho_{33}(t)] - \Omega_{\rm p}^*\rho_{13}(t)\}, \tag{B7}$$

and four equations represent the equations of motion for the population,

$$\dot{\rho}_{11}(t) = \gamma_{21}\rho_{22}(t) + \gamma_{31}\rho_{33}(t) + \gamma_{41}\rho_{44}(t) - \frac{i}{2}[\Omega_{\rm p}\rho_{41}(t) - \Omega_{\rm p}^*\rho_{14}(t)], \tag{B8}$$

$$\dot{\rho}_{22}(t) = -\gamma_{21}\rho_{22}(t) + \gamma_{32}\rho_{33}(t) + \gamma_{42}\rho_{44}(t) - \frac{i}{2}[-\Omega_{\rm c}^*\rho_{24}(t) + \Omega_{\rm c}\rho_{42}(t)], \tag{B9}$$

$$\dot{\rho}_{33}(t) = -\gamma_{31}\rho_{33}(t) - \gamma_{32}\rho_{33}(t) + \gamma_{43}\rho_{44}(t) - \frac{i}{2}[-\Omega_{\rm s}^*\rho_{34}(t) + \Omega_{\rm s}\rho_{43}(t)], \tag{B10}$$

$$\dot{\rho}_{44}(t) = -\gamma_4\rho_{44}(t) - \frac{i}{2}[\Omega_{\rm c}\rho_{24}(t) - \Omega_{\rm c}^*\rho_{42}(t) + \Omega_{\rm s}\rho_{34}(t) - \Omega_{\rm s}^*\rho_{43}(t) + \Omega_{\rm p}\rho_{14}(t) - \Omega_{\rm p}^*\rho_{41}(t)]. \tag{B11}$$

We now have the requisite equations of motion for the density-matrix elements to solve the dynamics.

APPENDIX C: ANALYTICAL STEADY-STATE SOLUTIONS

General analytical steady-state solutions for ρ_{14} and ρ_{34} are impossible without making assumptions or employing approximate conditions. Therefore, in our system we assume constant populations. This assumption makes the equations somewhat solvable analytically, as the equations of motion for population (B3) are effectively decoupled from the equations of motion for coherence (B2). We also assume that

$$|\Omega_{\rm c}|^2 \gg |\Omega_{\rm p}|^2, |\Omega_{\rm s}|^2 \tag{C1}$$

is always valid for all chosen values of $\Omega_{\rm c}$, $\Omega_{\rm p}$, and $\Omega_{\rm s}$. This assumption makes it possible to decouple the coherence ρ_{24}

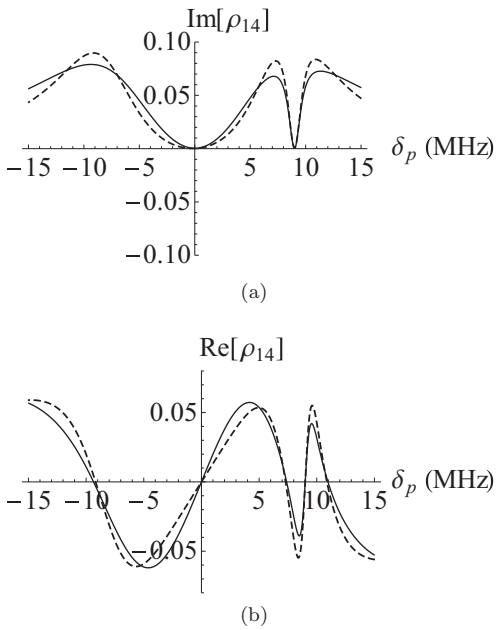

FIG. 5. (a) Im[ρ_{14}] and (b) Re[ρ_{14}] as a function of the probe-field detuning $\delta_{\rm p}$, with numerical (solid line) and analytical (dashed line) solutions, for $\gamma_4 = 18$ MHz, $\Omega_{\rm p} = \Omega_{\rm s} = 0.2\gamma_4$, $\Omega_{\rm c} = \gamma_4$, $\gamma_3 = 10$ kHz, $\gamma_2 = 40$ kHz, $\delta_{\rm s} = 9$ MHz, and $\delta_{\rm c} = 0$. For the case of the analytical solution we assume $\rho_{11} = \rho_{33} = 0.5$.

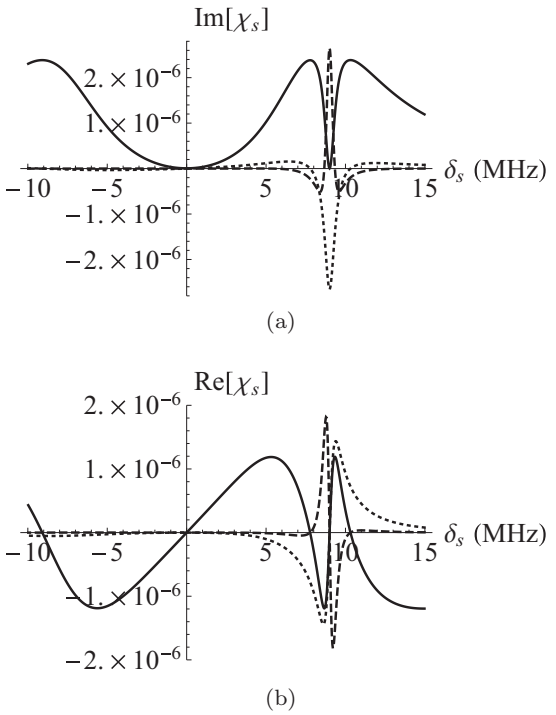

FIG. 6. (a) Im[$\chi_{\rm p}$] and (b) Re[$\chi_{\rm p}$] as a function of the probe-field detuning $\delta_{\rm p}$. The XPM term is represented by the dotted line, the SPM term is shown by the dashed line, and the linear term $\chi_{\rm s}^{(1)} \times 10^{-3}$ is given by the solid line, with $\gamma_4 = 18$ MHz, $\Omega_{\rm p} = 0.2\gamma_4$, $\Omega_{\rm c} = \gamma_4$, $\gamma_3 = 10$ kHz, $\gamma_2 = 40$ kHz, $\delta_{\rm p} = 9$ MHz, $\delta_{\rm c} = 0$, $d_{14} = d_{34} = 1.269 \times 10^{-29}$ C m, and $\mathcal{N} = 10^{12}$ cm^{-3}.

from other coherences, which is accomplished by eliminating $\Omega_{\rm p}\rho_{24}$ and $\Omega_{\rm s}^*\rho_{24}$ terms from $\dot{\rho}_{23}(t)$ and $\dot{\rho}_{12}(t)$ in (B2) and (B5), respectively, because their influence is weak compared to that of other terms.

Thus, the off-diagonal steady-state density-matrix element ρ_{14} can be calculated as

$$\rho_{14} = \Omega_{\rm p}\frac{i(\rho_{11}-\rho_{44}) + \frac{\Omega_{\rm s}}{\gamma_3 - 2i\delta_{\rm ps}}\rho_{43}}{\gamma_4 - 2i\delta_{\rm p} + \frac{|\Omega_{\rm c}|^2}{\gamma_2 - 2i\delta_{\rm pc}} + \frac{|\Omega_{\rm s}|^2}{\gamma_3 - 2i\delta_{\rm ps}}}, \tag{C2}$$

where

$$\rho_{43} = \Omega_{\rm s}^*\frac{-i(\rho_{33}-\rho_{44}) + \frac{\Omega_{\rm p}^*}{\gamma_3 - 2i\delta_{\rm ps}}\rho_{14}}{\Gamma_{43} + 2i\delta_{\rm s} + \frac{|\Omega_{\rm c}|^2}{\Gamma_{32} + 2i\delta_{\rm sc}}} \tag{C3}$$

is the optical response to the signal field for the $|4\rangle \rightarrow |3\rangle$ transition. We substitute Eq. (C3) into Eq. (C2) to obtain (4). Figure 5 shows the agreement between the analytical and numerical solutions. This analysis validates our analytical solution for optical property investigations.

APPENDIX D: SIGNAL-FIELD NONLINEAR OPTICAL PROPERTIES

Like in the probe-field case, we can write the effective optical susceptibility of the signal field as

$$\chi_{\rm s} = \chi_{\rm s}^{(1)} + \chi_{\rm s_{SPM}}^{(3)}|\boldsymbol{E}_{\rm s}|^2 + \chi_{\rm s_{XPM}}^{(3)}|\boldsymbol{E}_{\rm p}|^2, \tag{D1}$$

with

$$\chi_{\rm s}^{(1)} = \frac{i\eta_{\rm s}(\rho_{33}-\rho_{44})}{\Gamma_{43} - 2i\delta_{\rm s} + \frac{|\Omega_{\rm c}|^2}{\Gamma_{32} - 2i\delta_{\rm sc}} + \frac{|\Omega_{\rm p}|^2}{\gamma_3 + 2i\delta_{\rm ps}}} \tag{D2}$$

being the linear optical susceptibility at the signal-field frequency. As in the probe-field case, the linear absorption and dispersion of the signal field vanish at the center of the first and second EIT windows, as shown in Fig. 6.

The third-order nonlinear optical susceptibility appearing in the second term of Eq. (D1) can be written as

$$\chi_{\rm s_{SPM}}^{(3)} = \frac{i\eta_{\rm s_1}(\rho_{33}-\rho_{44})}{\left(\gamma_3 + 2i\delta_{\rm ps}\right)\left(\gamma_4 + 2i\delta_{\rm p} + \frac{|\Omega_{\rm c}|^2}{\gamma_2 + 2i\delta_{\rm pc}}\right)} \times \frac{1 - \frac{\Gamma_{43} - 2i\delta_{\rm s} + \frac{|\Omega_{\rm c}|^2}{\Gamma_{32} - 2i\delta_{\rm sc}}}{\Gamma_{43} - 2i\delta_{\rm s} + \frac{|\Omega_{\rm c}|^2}{\Gamma_{32} - 2i\delta_{\rm sc}} + \frac{|\Omega_{\rm p}|^2}{\gamma_3 + 2i\delta_{\rm ps}}}}{\Gamma_{43} - 2i\delta_{\rm s} + \frac{|\Omega_{\rm c}|^2}{\Gamma_{32} - 2i\delta_{\rm sc}} + \frac{|\Omega_{\rm p}|^2}{\gamma_3 + 2i\delta_{\rm ps}}}, \tag{D3}$$

with

$$\eta_{\rm s_1} = \frac{\mathcal{N}|\boldsymbol{d}_{43}|^4}{2\hbar^3\epsilon_0}. \tag{D4}$$

The imaginary part of the second term characterizes the two-photon absorption of the signal field, whereas the real part represents the self-action Kerr effect. The phase modulation of the signal field through the optical system by itself action can be calculated using

$$\phi_{\rm NL_{s_{SPM}}} = \frac{\omega_{\rm s}}{c} n_{\rm s_{SPM}}|\boldsymbol{E}_{\rm s}|^2 z_{\rm s}, \tag{D5}$$

where

$$n_{\mathrm{s_{SPM}}} = \frac{\mathrm{Re}\left[\chi^{(3)}_{\mathrm{s_{SPM}}}\right]}{2n_{\mathrm{s}}} \tag{D6}$$

is the second-order nonlinear refractive index, z_{s} is the propagation distance of the signal field through the optical medium, and

$$n_{\mathrm{s}} \approx 1 + \tfrac{1}{2}\mathrm{Re}\left[\chi^{(1)}_{\mathrm{s}}\right] \tag{D7}$$

is the linear index of refraction.

The third term on the right-hand side of Eq. (D1) depicts the cross-coupling effect between the probe and signal fields. The imaginary part of this term is responsible for producing stimulated Raman gain at the signal-field frequency [2] with energy detuning $\delta_{\mathrm{s}} = \delta_{\mathrm{p}}$ under the condition

$$\rho_{11}|\Omega_{\mathrm{p}}|^2 > \rho_{33}|\Omega_{\mathrm{s}}|^2. \tag{D8}$$

The real part of the third term on the right-hand side of Eq. (D1) represents the cross-coupling Kerr effect between the signal and probe fields, where the nonlinear optical susceptibility can be expressed as

$$\chi^{(3)}_{\mathrm{s_{XPM}}} = \frac{i\eta_{\mathrm{sp}}(\rho_{44}-\rho_{11})}{\left(\gamma_3 + 2i\delta_{\mathrm{ps}}\right)\left(\gamma_4 + 2i\delta_{\mathrm{p}} + \frac{|\Omega_{\mathrm{c}}|^2}{\gamma_2 + 2i\delta_{\mathrm{pc}}}\right)} \times \frac{1}{\Gamma_{43} - 2i\delta_{\mathrm{s}} + \frac{|\Omega_{\mathrm{c}}|^2}{\Gamma_{32}-2i\delta_{\mathrm{sc}}} + \frac{|\Omega_{\mathrm{p}}|^2}{\gamma_3+2i\delta_{\mathrm{ps}}}}. \tag{D9}$$

Modulation of the signal-field phase by the probe-field intensity through the nonlinear medium can be obtained using

$$\phi_{\mathrm{NL_{s_{XPM}}}} = \frac{\omega_{\mathrm{s}}}{c} n_{\mathrm{s_{XPM}}} \left|\boldsymbol{E}_{\mathrm{p}}\right|^2 z_{\mathrm{s}}, \tag{D10}$$

with

$$n_{\mathrm{s_{XPM}}} = \frac{\mathrm{Re}\left[\chi^{(3)}_{\mathrm{s_{XPM}}}\right]}{2n_{\mathrm{s}}} \tag{D11}$$

being the second-order nonlinear refractive index associated with the cross-coupling effect.

Similar to the probe-field case, the two-photon absorption of the signal field is overwhelmed by the gain of the signal field due to Raman scattering, which leads to no losses when $\Omega_{\mathrm{p}} = \Omega_{\mathrm{s}}$. Thus, XPM and SPM are not accompanied by linear or nonlinear absorption, as shown in Fig. 6(a).

APPENDIX E: VARIATION OF THE SIGNAL-FIELD NONLINEAR INDEX OF REFRACTION BY APPLIED FIELD DETUNINGS

Detuning the coupling field modifies the XPM and SPM values in the same way as in the case of the probe field, as shown in Fig. 7. Increasing or decreasing the coupling-field energy from the $|2\rangle \leftrightarrow |4\rangle$ transition energy results in displacing the XPM and SPM values from zero. Maximum displacement is achieved for $\delta_{\mathrm{c}} = \frac{\delta_{\mathrm{p}}}{2}$.

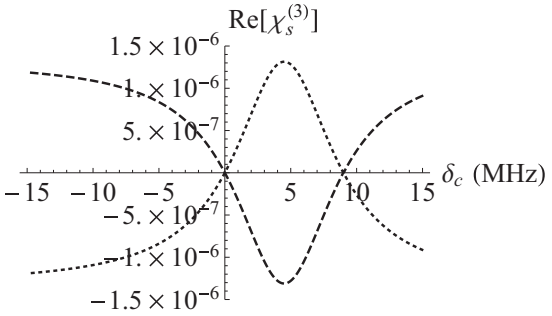

FIG. 7. $\mathrm{Re}[\chi_{\mathrm{s}}^{(3)}]$ with XPM (dotted line) and SPM (dashed line) as a function of the coupling detuning δ_{c} at the center of the second EIT window when $\delta_{\mathrm{s}} = \delta_{\mathrm{p}} = 9$ MHz. Other parameters are $\gamma_4 = 18$ MHz, $\Omega_{\mathrm{s}} = 0.2\gamma_4$, $\Omega_{\mathrm{c}} = \gamma_4$, $\gamma_3 = 10$ kHz, $\gamma_2 = 40$ kHz, $d_{14} = d_{34} = 1.269\times10^{-29}$ C m, and $\mathcal{N} = 10^{12}$ cm^{-3}.

Detuning the coupling field plays an important role in modifying the XPM and SPM values at the center of the second EIT window. Figure 3 demonstrates the variation of XPM and SPM as a function of coupling-field detuning. The nonlinear dispersion response including XPM and SPM vanishes for a resonant coupling field. However, detuning the coupling field to a lower or a higher energy value than the $|2\rangle \leftrightarrow |4\rangle$ transition energy displaces the XPM and SPM values from zero, and they reach their maximum values for $\delta_{\mathrm{c}} = \frac{\delta_{\mathrm{s}}}{2}$.

We obtain an approximation of $\mathrm{Re}[\chi^{(3)}_{\mathrm{s_{XPM}}}]$ as a function of coupling-field detuning for $\delta_{\mathrm{s}} = \delta_{\mathrm{s}}$, in a way similar to that of result (23), as

$$\mathrm{Re}\left[\chi^{(3)}_{\mathrm{s_{XPM}}}\right] \approx \frac{2\eta_{\mathrm{sp}}(\rho_{44}-\rho_{11})\delta_{\mathrm{pc}}\left(\delta_{\mathrm{p}} - \frac{|\Omega_{\mathrm{c}}|^2}{4\delta_{\mathrm{pc}}}\right)}{|\Omega_{\mathrm{p}}|^2\left[\delta_{\mathrm{pc}}^2\gamma_4 3^2 + 4\left(\delta_{\mathrm{pc}}\delta_{\mathrm{p}} - \frac{|\Omega_{\mathrm{c}}|^2}{4}\right)^2\right]}. \tag{E1}$$

Thus, XPM vanishes for $\delta_{\mathrm{p}} = \delta_{\mathrm{c}}$ and for

$$\delta_{\mathrm{p}} - \frac{|\Omega_{\mathrm{c}}|^2}{4\delta_{\mathrm{pc}}} = 0, \tag{E2}$$

which are exactly the same conditions as for vanishing SPM and XPM of the probe field at $\delta_{\mathrm{p}} = \delta_{\mathrm{s}}$.

Therefore, to enhance the nonlinear index of refraction of the signal field, the probe field must not be in resonance with the dressed state $|3\rangle \leftrightarrow |\pm\rangle$. This result can be generalized to the case of SPM, as analyzing $\mathrm{Re}[\chi^{(3)}_{\mathrm{s_{SPM}}}]$ leads to the same result.

[1] S. E. Harris, Phys. Today **50**(7), 36 (1997).
[2] H. M. M. Alotaibi and B. C. Sanders, Phys. Rev. A **89**, 021802 (2014).
[3] A. Imamoğlu and S. E. Harris, Opt. Lett. **14**, 1344 (1989).
[4] S. E. Harris, Phys. Rev. Lett. **62**, 1033 (1989).
[5] O. Kocharovskaya, Phys. Rep. **219**, 175 (1992).
[6] O. Kocharovskaya, Hyperfine Interact. **107**, 187 (1997).
[7] J. Mompart and R. Corbalan, J. Opt. B **2**, R7 (2000).
[8] G. Vemuri and G. S. Agarwal, Phys. Rev. A **53**, 1060 (1996).
[9] K. Hakuta, L. Marmet, and B. P. Stoicheff, Phys. Rev. Lett. **66**, 596 (1991).
[10] S. P. Tewari and G. S. Agarwal, Phys. Rev. Lett. **56**, 1811 (1986).

[11] S. E. Harris, J. E. Field, and A. Imamoğlu, Phys. Rev. Lett. **64**, 1107 (1990).
[12] A. J. Merriam, S. J. Sharpe, M. Shverdin, D. Manuszak, G. Y. Yin, and S. E. Harris, Phys. Rev. Lett. **84**, 5308 (2000).
[13] L. V. Hau, S. E. Harris, Z. Dutton, and C. H. Behroozi, Nature (Londen) **397**, 594 (1999).
[14] S. E. Harris and L. V. Hau, Phys. Rev. Lett. **82**, 4611 (1999).
[15] M. M. Kash, V. A. Sautenkov, A. S. Zibrov, L. Hollberg, G. R. Welch, M. D. Lukin, Y. Rostovtsev, E. S. Fry, and M. O. Scully, Phys. Rev. Lett. **82**, 5229 (1999).
[16] A. MacRae, G. Campbell, and A. I. Lvovsky, Opt. Lett. **33**, 2659 (2008).
[17] H. M. M. Alotaibi and B. C. Sanders, Phys. Rev. A **91**, 043817 (2015).
[18] Y. Han, J. Xiao, Y. Liu, C. Zhang, H. Wang, M. Xiao, and K. Peng, Phys. Rev. A **77**, 023824 (2008).
[19] J. Kou, R. G. Wan, Z. H. Kang, H. H. Wang, L. Jiang, X. J. Zhang, Y. Jiang, and J. Y. Gao, J. Opt. Soc. Am. B **27**, 2035 (2010).
[20] B.-W. Shiau, M.-C. Wu, C.-C. Lin, and Y.-C. Chen, Phys. Rev. Lett. **106**, 193006 (2011).
[21] Rajitha K. V., T. N. Dey, J. Evers, and M. Kiffner, Phys. Rev. A **92**, 023840 (2015).
[22] R. S. Bennink, R. W. Boyd, C. R. Stroud, and V. Wong, Phys. Rev. A **63**, 033804 (2001).
[23] H. Schmidt and A. Imamoğlu, Opt. Lett. **21**, 1936 (1996).
[24] S. Rebić, D. Vitali, C. Ottaviani, P. Tombesi, M. Artoni, F. Cataliotti, and R. Corbalán, Phys. Rev. A **70**, 032317 (2004).
[25] A. Joshi and M. Xiao, Phys. Rev. A **72**, 062319 (2005).
[26] S. E. Harris and A. V. Sokolov, Phys. Rev. Lett. **81**, 2894 (1998).
[27] I. Friedler, G. Kurizki, O. Cohen, and M. Segev, Opt. Lett. **30**, 3374 (2005).
[28] J. Soumendu and S. Konar, Phys. Lett. A **362**, 435 (2007).
[29] J. P. Poizat and P. Grangier, Phys. Rev. Lett. **70**, 271 (1993).
[30] N. Yueping, G. Shangqing, L. Ruxin, X. Zhizhan, and X. Liang, Opt. Lett. **30**, 3371 (2005).
[31] Z.-B. Wang, K.-P. Marzlin, and B. C. Sanders, Phys. Rev. Lett. **97**, 063901 (2006).
[32] C. Ottaviani, S. Rebić, D. Vitali, and P. Tombesi, Phys. Rev. A **73**, 010301 (2006).
[33] X. K. Dinh, L. V. Doai, H. S. Doan, and H. B. Nguyen, J. Opt. Soc. Am. B **31**, 1330 (2014).
[34] X. Yang and S. Zhu, Phys. Rev. A **78**, 023818 (2008).
[35] D. Wang and J. Zhang (unpublished).
[36] R. W. Boyd, *Nonlinear Optics*, 3rd ed. (Academic, Burlington, MA, 2008).
[37] J. Gea-Banacloche, Y.-q. Li, S.-z. Jin, and M. Xiao, Phys. Rev. A **51**, 576 (1995).
[38] C. Y. Ye and A. S. Zibrov, Phys. Rev. A **65**, 023806 (2002).
[39] W. M. Kirk and C.-T. Claude, *Annual Review of Cold Atoms and Molecules* (World Scientific, Singapore, 2013), Vol. 1.